Modeling the Nonlinear Response of Multitones With Uncorrelated Phase

Frank P. Hart, *Member, IEEE*, and Michael B. Steer, *Fellow, IEEE*

***Abstract*—Traditional simulation approaches for predicting the frequency-domain response of nonlinear devices to multiple tone excitation enforce correlation of the phases of the individual tones. This is the case with time-domain simulators and transform-based schemes such as Harmonic balance as the waveform must be single valued, thus enforcing correlation. Previous efforts in frequency-domain simulators using the arithmetic operator method (AOM) also produced results in good agreement with measurements for correlated-phase input signals. Here, the AOM is applied to directly determine the spectral response of nonlinear systems to excitation by multiple uncorrelated tones in a single simulation. Verification is provided using measurements of a nonlinear amplifier excited by 15 independent tones and comparison to the average of the ensemble of results from multiple correlated-phase simulations.**

***Index Terms*—Arithmetic operator method (AOM), computer-aided analysis, multitone signals, nonlinear amplifiers, uncorrelated phase.**

I. Introduction

ONE OF the fundamental questions in RF and microwave simulation is whether or not the response of nonlinear systems to tones that are uncorrelated is correctly captured in simulation. Many multitone test systems also produce correlated tones through deliberate phase locking, indirect locking whereby the tones maintain close phase correlation during a measurement sample, or through digital synthesis. Uncorrelated tones more accurately describe real-world situations where the individual tones are often combined from sources that are not localized. A simulation scheme that explicitly or implicitly requires a time-domain representation enforces correlation of the tones. In the case of time-domain analysis in a transient circuit simulator, only relatively short intervals can be modeled in a reasonable time, i.e., it is not possible to perform a simulation for the time required to slowly dither the phases of the individual tones. In harmonic balance (HB) methods, the unknowns solved for are the amplitude and phases of individual phasors describing the states at the nodes of a nonlinear circuit partition that interface to a linear circuit partition. If the excitation tones are uncorrelated, then within a single simulation, the coherent summing of nonlinear tone interactions gives resulting vector sums that nearly vanish at some frequencies while expanding to large magnitudes at others due to coincidental phase alignment. Thus, for accurate results in the case of uncorrelated phase inputs, it is typical to perform a large number of simulations and randomly vary the initial phases of the excitation tones. The phasor responses from the ensemble of simulations are then averaged.

Most of the literature concerning the nonlinear analysis of RF circuits deals with small numbers of necessarily correlated input tones. Typical commercial HB simulators limit the source stimulus to 12 tones [1]. Rizzoli *et al.* [2]–[4] used an uncorrelated time-domain stimulus to report results of HB simulations on a narrowband digitally modulated input signal comprising a sequence of 1024 uncorrelated bits at a baseband rate of 48.6 kb/s. In these reports, each simulation is completed in 1 h or less, and a large number of sampling locations are possible due to innovative simplifications in the numerical processing of the Newton iterates. In a later publication [5], a somewhat broader band wideband code division multiple access (W-CDMA) signal was processed through a spline-based behavioral model, which required 27 h to construct, but only 35 s to deploy in a simulation producing 160 000 output samples.

The purpose of this paper is to introduce a nonlinear analysis scheme that models the response of a nonlinear system excited by multiple uncorrelated tones. The work here was motivated by the problem of simulating systems with very many tones, as in the cable-TV industry, where the tones, i.e., carrier frequencies, are not commensurably related [6]. The most recent successful modeling effort supported by measurements reported results based upon a power series model with a stimulus of only six carrier frequencies [7]. This study is a continuation of an effort to develop a theory of nonlinear circuit and system analysis that is entirely based in the frequency domain. When simulating solely in the frequency domain, it is possible to construct an environment that preserves all of the phasor content created at each order of nonlinearity. In turn, this facilitates the accurate computation of average power levels for uncorrelated inputs by squaring the magnitude of each phasor and performing a sum of the squares, i.e., by summing the power of individual phasors rather than finding the power of a vectorial sum of phasors.

The analysis method described here is based on the arithmetic operator method (AOM), which performs nonlinear analysis entirely in the frequency domain. AOM has been used successfully within the microwave community for nearly two decades for frequency-domain analysis of nonlinear systems with correlated-phase stimulus signals. Many of the advantages inherent to AOM were first reported by Haywood and Chow [8], but of particular utility is the avoidance of repeated forward and inverse

Manuscript received April 16, 2007; revised July 5, 2007. This work was supported by the U.S. Army Research Laboratory and by the U.S. Army Research Office on Standoff Inverse Analysis and Manipulation of Electronic Systems under Grant W911NF-05-1-0337.

The authors are with the Department of Electrical and Computer Engineering, North Carolina State University, Raleigh, NC 27695-7914 USA (e-mail: fphart@eos.ncsu.edu; mbs@ncsu.edu).

Color versions of one or more of the figures in this paper are available online at http://ieeexplore.ieee.org.

Digital Object Identifier 10.1109/TMTT.2007.906462

0018-9480/$25.00 © 2007 IEEE

Authorized licensed use limited to: North Carolina State University. Downloaded on February 2, 2009 at 13:52 from IEEE Xplore. Restrictions apply.

Fourier transforms inherent to HB methods and the ability to operate on arbitrarily spaced discrete input spectra. The first functioning circuit simulator based upon AOM was described by Chang *et al.* [9]; this environment was enhanced later to include transcendental function nonlinearities [10]. Another circuit simulator environment inspired by Chang's study was developed shortly thereafter [11], and developments within that environment included multivariate rational polynomial modeling [12] culminating in a large-signal model for a pseudomorphic HEMT (pHEMT) [13]. A concurrent development by de Carvalho and Pedro [14] consciously sacrificed the ability to arbitrarily space the discrete input spectral content in favor of simplicity of construction of the simulation environment [15]. Nevertheless, notable results were produced for cases of a noise power input consisting of 11 tones [16] and a 32-tone input approximating a partial television transmission scheme [17]. In the case of the noise power test, however, multiple simulations were done to vary the phase of the 11 input tones; thus, the environment apparently enforces correlation. de Carvalho and Pedro later modified their environment to validate Volterra analysis techniques they developed for predicting the adjacent channel and co-channel intermodulation (IM) response to multitone inputs with correlated and uncorrelated phases [18]. Since their frequency indexing scheme does not enable the preservation of different nonlinearly created phasors that map to the same numerical frequency, they began with the assumption that all input spectral content was uncorrelated and simply superposed the power contributions of spectral content in their computations, thus ending with a valid power computation despite not preserving the phasor content. The environment used to produce the results presented in this paper differs from that of de Carvalho and Pedro in that it preserves nonlinearly created phasor content, thus it is well suited for handling both correlated and uncorrelated phase multitone input signals.

II. Computer-Aided Modeling Environment

The applicability of the AOM to model nonlinear systems depends upon two factors. First, the input to the system under consideration must be composed of discrete spectra. Second, the transfer function of the system under consideration must be reducible to a rational polynomial form with transcendental functions permitted, provided that their infinite series representation may be truncated. Although the second factor has been viewed in some quarters as an inherent limitation of the AOM, it should be noted that the numerical evaluation of transcendental functions in digital computers is accomplished via either limiting sums of Taylor series [19] or by iterative methods embedded in numeric coprocessing hardware [20]. Thus, the truncation of the evaluated transcendental function is hidden from the user of the numerical computing environment when methods other than the AOM are used.

The AOM Toolbox is a new behavioral modeling implementation of the AOM that exploits MATLAB's sparse matrix handling capabilities [21]. The modeling environment is implemented as a set of callable functions in the MATLAB toolbox form. A typical MATLAB script using the toolbox performs the following actions, which will be described in further detail in Sections II-A–E:

- define the input signal amplitude, phase, and frequency vectors;
- call the function to create the basic IM product description (BIPD) table;
- call the function to create the input spectral vector;
- call the function to create the spectrum mapping table;
- call the function to create the spectrum transform matrix;
- call the function to evaluate the transfer function and produce the output spectral vector;
- perform any further output data processing, e.g., plotting.

A. Input Signal

Let $x(t)$ correspond to a time-domain input function comprised of a sum of Q sinusoids as defined similarly in [22]

$$x(t) = \sum_{q=1}^{Q} |X_q| \cos(2\pi f_q t + \phi_q) \tag{1}$$

$$= \frac{1}{2}\sum_{q=1}^{Q} X_q e^{\jmath 2\pi f_q t} + \frac{1}{2}\sum_{q=1}^{Q} X_q^* e^{-\jmath 2\pi f_q t} \tag{2}$$

where $\jmath$ is the imaginary number and $|X_q|$, f_q, and ϕ_q are the amplitude, frequency, and phase offsets, respectively, of each signal component, and where X_q is the phasor representation of the amplitude and phase, thus, $X_q = |X_q| e^{\jmath\phi_q}$. X_q^* is also the complex conjugate of X_q. In the frequency domain, the Fourier transform (denoted $\overset{\mathfrak{F}}{\Longrightarrow}$) of the complex exponentials in $x(t)$ are Dirac delta functions [23], thus,

$$x(t) \overset{\mathfrak{F}}{\Longrightarrow} X(f) = \frac{1}{2}\sum_{q=1}^{Q} \left[X_q \delta(f - f_q) + X_q^* \delta(f + f_q)\right]. \tag{3}$$

where the first Dirac delta term corresponds to the positive portion of the spectrum and the second term corresponds to the negative portion of the spectrum. Since $X(f)$ is discrete, it can be cast in the form of a vector $\mathbf{X}$, thus permitting the use of linear algebra computational techniques. For real-valued signals, it is possible to exploit the conjugate symmetry of the signal by using only the positive portion of the spectrum. Note also that the input frequency locations $f_1 \ldots f_Q$ may be conveniently described as a vector $\mathbf{f} = [f_1 \ldots f_Q]^{\mathrm{T}} \in \mathbb{R}^{Q\times 1}$.

B. BIPD Table

Given an input signal, as defined in Section II-A, and a transfer function with a maximum order of nonlinearity N, the BIPD [9], [10] table uniquely identifies the location of all output spectral content in the form of a vector space of integer tuples denoting instances of input spectral content. In essence, the BIPD represents a further decomposition of the input domain, the numerical frequency domain, which then facilitates a similar decomposition of the output domain into phasor contents with a one-to-one relationship with the BIPD. Note that the construction of the BIPD table does not depend upon whether the transfer function has memory or not, but depends only upon its order of nonlinearity. For an input signal composed of Q sinusoids, a distinct BIPD table entry will then take the form of a row vector $\boldsymbol{\nu}^{\mathrm{T}} \in \mathbb{I}^{1\times Q}$. The table is initialized to a $Q \times Q$ identity matrix to account for the linear

Authorized licensed use limited to: North Carolina State University. Downloaded on February 2, 2009 at 13:52 from IEEE Xplore. Restrictions apply.

response $(n = 1)$, and construction of the table thereafter is a combinatorial process at each order of nonlinearity from $n = 2$ to N. Table entries for each order of nonlinearity are built by adding and subtracting upper circulant shifted versions of the identity matrix (through a total of Q shifts) to the BIPD table entries for order $n - 1$. In this process, negative frequency weightings (corresponding to subtractive IM) are permitted, but the resulting output frequency, given by the dot product $\boldsymbol{\nu}^{\mathrm{T}} \cdot \mathbf{f}$, must be nonnegative, and the 1-norm of $\boldsymbol{\nu}^{\mathrm{T}}$ (defined as $\|\boldsymbol{\nu}\|_1 = \sum_{i=1}^{Q} |\nu_i|$), $\|\boldsymbol{\nu}\|_1$, must be equal to n. For the case of $Q > N$, the number of output frequencies created at each order of nonlinearity, i.e., n, is bound by the following relationship:

$$\mathcal{V}_n = 2^{(n-1)} \left[\binom{Q+n-1}{n} - \sum_{nz=1}^{n} \binom{Q+nz-1}{nz} \right] + \sum_{nz=1}^{n} 2^{(nz-1)} \binom{Q+nz-1}{nz} \quad (4)$$

where nz denotes the number of nonzero tuples in BIPD vectors. The total number of nonnegative output frequencies created, ν, is the sum over all n plus 1 to account for dc, the 0 vector

$$\mathcal{V} = 1 + \sum_{n=1}^{N} \mathcal{V}_n. \quad (5)$$

Equation (4) is an application of the inclusion–exclusion principle [24] from combinatorics. In the case of estimating the number of unique BIPDs with nonnegative frequencies, the binomial expression $\binom{Q+n-1}{n}$ appearing in (4) furnishes a gross overestimate because the sign weighting factor $2^{(n-1)}$ assumes that each of n tuples is nonzero. The other factors in (4) account for those overestimates.

Note that while all BIPD table entries are unique, many of them may map to the same numerical frequency when input frequencies are commensurate (but uncorrelated). The ability of the AOM to discern the existence of equal-frequency spectral content with different BIPD vectors will be shown (see Table I) to be critical to its ability to predict the average power response of a nonlinearity to uncorrelated phase input tones.

C. Spectral Vector

Since each entry in the BIPD table identifies unique output spectral content, there is a one-to-one correspondence between BIPD table entries and the output phasors. A vector constructed so that its phasor content has this one-to-one correspondence with the BIPD table is a *spectral vector*. When the input signal is cast using the same vector space definition as the output signal, it becomes possible to use matrix-vector arithmetic and square matrices to transform (i.e., perform convolution on) the input signal to produce the output. Input signals in spectral vector form will customarily be denoted as $\mathbf{X}$, while output signals will be denoted as $\mathbf{Y}$. Using the BIPD table, an AOM Toolbox function casts the user's input signal in spectral vector form for further use.

TABLE I
NUMBERS OF PHASORS AVERAGED AT ADJACENT-BAND IM FREQUENCIES

Frequency (MHz)	Number of Phasors	Frequency (MHz)	Number of Phasors
415	1	433	718
416	2	434	817
417	5	435	917
418	9	436	1022
419	16	437	1125
420	25	438	1229
421	39	439	1327
422	56	440	1420
423	80	441	1502
424	109	442	1572
425	147	443	1715
426	192	444	1775
427	249	445	1824
428	315	446	1875
429	382	447	1910
430	459	448	1943
431	538	449	1957
432	627	450	1967

D. Spectrum Mapping Table and Spectrum Transform Matrix

Consider the *atomic multiplication* achieved by convolving the input signal $X(f)$ from (3) with itself at two arbitrary frequencies f_{q1} and f_{q2}

$$X(f_{q1}) \cdot X(f_{q2}) = \frac{1}{4} X_{q1} X_{q2} e^{\jmath(\phi_{q1}+\phi_{q2})} \delta\left[f - (f_{q1} + f_{q2})\right]. \quad (6)$$

Discrete convolution involves summing a series of atomic multiplications of this sort. Focusing on the Dirac delta function, notice that the effect of the convolution is to create new spectral content. When $f_{q1} = f_{q2}$, the new spectral content is a harmonic. Otherwise, it is IM. In either case, the result of discrete convolution mixing of incommensurate frequencies is another set of Dirac delta functions. To generalize, the nonlinear mixing of two entries in the BIPD table would result in a Dirac delta function $\delta[f - (\boldsymbol{\nu}_1^{\mathrm{T}} \cdot \mathbf{f} + \boldsymbol{\nu}_2^{\mathrm{T}} \cdot \mathbf{f})] = \delta[f - (\boldsymbol{\nu}_1^{\mathrm{T}} + \boldsymbol{\nu}_2^{\mathrm{T}}) \cdot \mathbf{f}]$, where ν_1 and ν_2 are the $1 \times Q$ vectors of integer frequency weightings. The algorithm that produces the spectrum mapping table identifies the location of nonzero content in a spectrum transform matrix by performing the BIPD additions (i.e., doing the frequency addition portion of the discrete convolution) and subtractions (to account for subtractive IM), assuring that the sum of the 1-norms of the BIPDs is less than or equal to the maximum nonlinear order, and checking that the resulting frequency is positive. If the outcome of these checks is affirmative, an entry is made in the spectrum mapping table, a table that facilitates the construction of the spectrum transform matrix.

The spectrum transform matrix is built such that its entries will achieve discrete convolution of a vector of phasors with itself. Note that even unusual mixing instances are handled with ease. For example, consider the case of the unit vector BIPDs $\boldsymbol{\nu}_1^{\mathrm{T}}$ and $\boldsymbol{\nu}_2^{\mathrm{T}}$ corresponding to input frequencies f_{q1} and f_{q2}, respectively, and let $\boldsymbol{\nu}_3^{\mathrm{T}} = \boldsymbol{\nu}_1^{\mathrm{T}} - \boldsymbol{\nu}_2^{\mathrm{T}}$ be a second-order BIPD. The third-order desensitizing mixture of $\boldsymbol{\nu}_3^{\mathrm{T}}$ and $\boldsymbol{\nu}_2^{\mathrm{T}}$ will then

Authorized licensed use limited to: North Carolina State University. Downloaded on February 2, 2009 at 13:52 from IEEE Xplore. Restrictions apply.

map to $\boldsymbol{\nu}_1^{\mathrm{T}}$, but since this mixing occurs at the third order, the mixing output will be recorded in a spectral vector for the third-order nonlinearity (as described in Section II-E), thus leaving the linear response phasor unaffected. See [25], [26] for details of the table and matrix construction. One recent improvement in the algorithm for computing the spectrum mapping table is reflected in the AOM Toolbox. Given a BIPD table with $\mathcal{V}$ entries as in (5), the algorithm described in [25] requires $\mathcal{O}(\mathcal{V}^3)$ operations to compute the spectrum mapping table. This has been reduced to $\mathcal{O}(\mathcal{V}^2)$ in the AOM Toolbox, which aligns with the theoretical expectation for the operation count to perform a discrete convolution [27].

There are AOM Toolbox functions for computing both the spectrum mapping table and spectrum transform matrix. The spectrum mapping table may be computed independently of the input spectral vector, thus allowing one spectrum mapping table to be reused for multiple solutions of a modeling problem with different input spectral vectors. The spectrum transform matrix, however, requires the use of the input spectral vector for its construction and must be computed for each unique input spectral vector.

E. Transfer Function

Let $x(t)$ be defined as in Section II-A, and recall from the theory of Fourier transforms [28] that repeated multiplication of time-domain functions corresponds to repeated convolution in the frequency domain, i.e.,

$$[x(t)]^n \stackrel{\mathfrak{F}}{\Longrightarrow} \underbrace{X(f) * X(f) * \cdots * X(f)}_{n \text{ times}}. \tag{7}$$

Consider the simple case of a second-order nonlinearity $y(t) = [x(t)]^2$, thus, $Y(f) = X(f) * X(f)$. Since $X(f)$ can be described in spectral vector form $\mathbf{X}$, the convolution operation can be recast in a matrix-vector form so that

$$Y(f) = X(f) * X(f) \equiv \mathbf{Y} = \mathbf{T}_x \mathbf{X} \tag{8}$$

where $\mathbf{T}_x$ is the spectrum transform matrix that produces the convolution result $X(f) * X(f)$ when it is right multiplied by $\mathbf{X}$. Thus, note that while a nonlinear system is being modeled, the computation is done using linear algebra [29].

Generalizing the previous example, let $y(t)$ be a memoryless polynomial time-domain transfer function

$$y(t) = a_0 + a_1 x(t) + a_2 [x(t)]^2 + \cdots + a_N [x(t)]^N \tag{9}$$

$$= \sum_{n=0}^{N} a_n [x(t)]^n \tag{10}$$

where a_n are real coefficients. Expressing $y(t)$ in the frequency domain, using the spectral vector representation so that $y(t) \stackrel{\mathfrak{F}}{\Longrightarrow} \mathbf{Y}$ and substituting (7) and (8) into the transform of (10),

$$\mathbf{Y} = a_0 \mathbf{e}_{\mathrm{DC}} + a_1 \mathbf{X} + a_2 \mathbf{T}_x \mathbf{X} + \cdots + a_N \mathbf{T}_x^{N-1} \mathbf{X} \tag{11}$$

$$= a_0 \mathbf{e}_{\mathrm{DC}} + \sum_{n=1}^{N} a_n \mathbf{T}_x^{n-1} \mathbf{X} \tag{12}$$

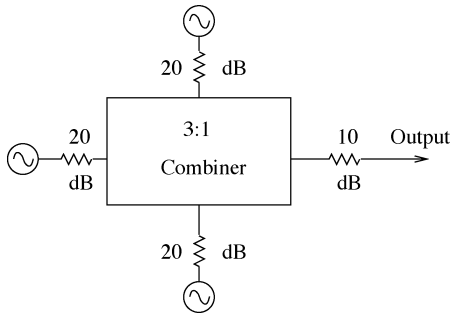

Fig. 1. Simplified block diagram of a three-oscillator assembly.

where $a_0 \mathbf{e}_{\mathrm{DC}}$ captures the constant (dc) part of the transfer function. Here, $\mathbf{e}_{\mathrm{DC}}$ is a unit vector of the same length as the spectral vectors $\mathbf{X}$ and $\mathbf{Y}$ with a 1 in the element reserved for constant (dc) spectral content and 0 elsewhere. The AOM Toolbox toolbox function for evaluating the transfer function returns an output spectral vector for the linear response and each order of nonlinearity, thus making possible the preservation of all of the nonlinearly created spectral content at each BIPD, including the example third-order desensitization term described in Section II-D. It should be noted here that the computation of the output spectral vector is accomplished entirely through the repeated convolution in (12) and not through the use of combinatorial computations of the sort found in [18] and [22]. Use of combinatorial algorithms in the AOM Toolbox is limited to the toolbox function used to construct the BIPD table.

III. Measurement Apparatus

A. Uncorrelated Phase Multitone Signal Generator

An uncorrelated phase multitone signal generator was created from an ensemble of five assemblies with each assembly containing three oscillators created from off-the-shelf parts. A block diagram of the three-tone assembly is shown in Fig. 1. An unusual aspect of the assembly is that the voltage-controlled oscillators are not controlled within phase-locked loops, but instead have their output frequencies set by simple variable resistance networks that permit a tuning range from approximately 410–490 MHz. The presence of 20-dB attenuators on each oscillator output, as shown in Fig. 1, is necessary to sufficiently isolate each oscillator from injection pulling [30] by the others. When the oscillators are spaced at least 1 MHz apart, the artifacts of injection pulling are observed to be below -90 dBm when a 10-dB attenuator is included at the assembly's combiner output. Despite lack of phase locking, it was found that the standard deviation of the stabilized oscillation frequency was less than 30 kHz when the assembly was housed in a *crude oven*—a well-sealed cardboard shipping box with a plastic sheeting lid—that typically reached a steady-state quiescent thermal environment approximately 0.5 h after operating power was applied. The outputs of five of these boxed assemblies are conducted via 0.5-m segments of subminiature A (SMA) cables, combined, then low-pass filtered to block harmonics of the oscillator outputs from further transmission. A block diagram of the complete multitone system is shown in Fig. 2.

Authorized licensed use limited to: North Carolina State University. Downloaded on February 2, 2009 at 13:52 from IEEE Xplore. Restrictions apply.

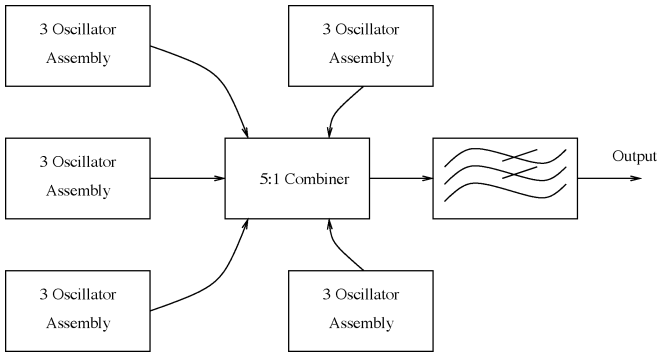

Fig. 2. Block diagram of the multitone system comprised of five three-tone assemblies.

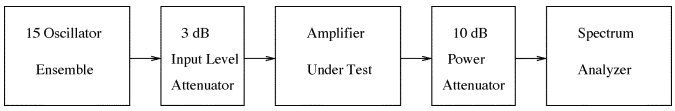

Fig. 3. Block diagram of the laboratory setup.

B. Laboratory Equipment Setup

A block diagram of the laboratory setup is shown in Fig. 3. For this work, the 15 oscillators of the multitone system were set to 1-MHz nominal increments between 443–457 MHz. The input attenuator permits adjustment of the input power level seen by the amplifier under test, and the power attenuator on the amplifier output protects the spectrum analyzer from input overload damage. For the purposes of the work performed here, the input attenuator value is selected such that peak power of the 15 tones (assuming perfect phase alignment) at the amplifier input is never greater than -4 dBm. A 0.6-m segment of SMA cable connects the input attenuator to the amplifier under test. Measurements were taken with a 3-dB input attenuator and a 10-dB 20-W power attenuator. The amplifier under test is a Mini-Circuits ZHL-5W-1 [31], a class-A amplifier with a frequency response between 5–500 MHz and an approximate gain of 45 dB in the vicinity of the 450-MHz center frequency of operation. The amplifier output connects to the power attenuator via a 1-m segment of SMA cable, and the power attenuator is directly connected to the spectrum analyzer. The spectrum analyzer is an HP-8565E operating under the control of a LabView Virtual Instrument that was developed to support this study. Each measurement sweep of the HP-8565E captures 601 points of data.

IV. Results and Discussion

The transfer function for the amplifier under test was previously extracted using narrowband extraction techniques with two tones in the vicinity of 450 MHz [32], [33]. The extracted transfer function was a polynomial with nonzero odd-order coefficients up to the 15th order and valid for input signals with a total input power under 0 dBm. For use in the modeling environment here, the transfer function was truncated to the fifth order; i.e., N in (12) was set to 5, thus discarding the odd-order terms from 7 to 15—terms that were expected to produce output power levels well below the noise floor and, hence, have little

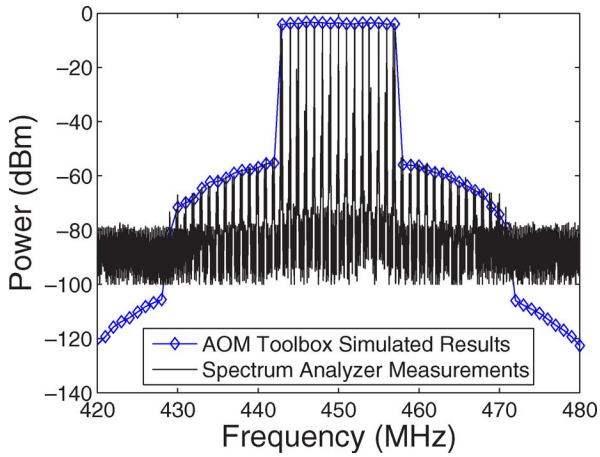

Fig. 4. Simulated and measured results for adjacent-band IM.

incremental effect upon the simulated results. Two IM analysis scenarios were considered. The first scenario considered the adjacent-band IM distortion in the vicinity of a collection of 15 uncorrelated phase carrier signals. The second scenario considered the in-band IM distortion produced by the nonlinear amplification of a set of 14 uncorrelated phase carrier signals in the immediate vicinity of one carrier, the center frequency carrier, which had been turned off. This is a common measurement scenario in the cable television industry [34], and it is one for which the industry is seeking predictive computer-aided analysis tools.

A. Adjacent-Band IM Analysis Example

Fig. 4 shows the results of a typical adjacent-band IM measurement compared to the results simulated by the computer-aided environment when power computations assume that input carriers consist of uncorrelated phases, i.e., the power computation is done by squaring the magnitude of all phasors appearing at the same numerical frequency and summing in lieu of the typical method of assuming that phasors are correlated and squaring the magnitude of a coherent or vectorial sum. Good agreement can be seen in the linear and adjacent IM bands of Fig. 4 with the possible exception of the far edges of the IM bands around 430 and 470 MHz. (The simulated fifth-order IM falls well below the noise floor of the measuring equipment, thus justifying the decision to truncate the transfer function in the computer model.) Note that when the numbers of input tones (or carriers) is larger than a few, the number of nonlinearly created phasors appearing at the same frequency can become quite large. Table I shows the number of unique phasors created (by virtue of different BIPD vectors) for each of the frequencies from 415 to 450 MHz. (Due to transfer function symmetry, a reversed version of the table gives the numbers of nonlinearly created phasors from 450 to 485 MHz.) It can be seen that in the adjacent IM band, there are cases where more than 1000 phasors are being averaged so it should be expected that power computations based on coherent or vectorial sums due to enforced correlation will vary greatly from power computations that assume uncorrelated phases.

The simulated results of Fig. 4 can be contrasted with results typical of that for environments that enforce correlation

Authorized licensed use limited to: North Carolina State University. Downloaded on February 2, 2009 at 13:52 from IEEE Xplore. Restrictions apply.

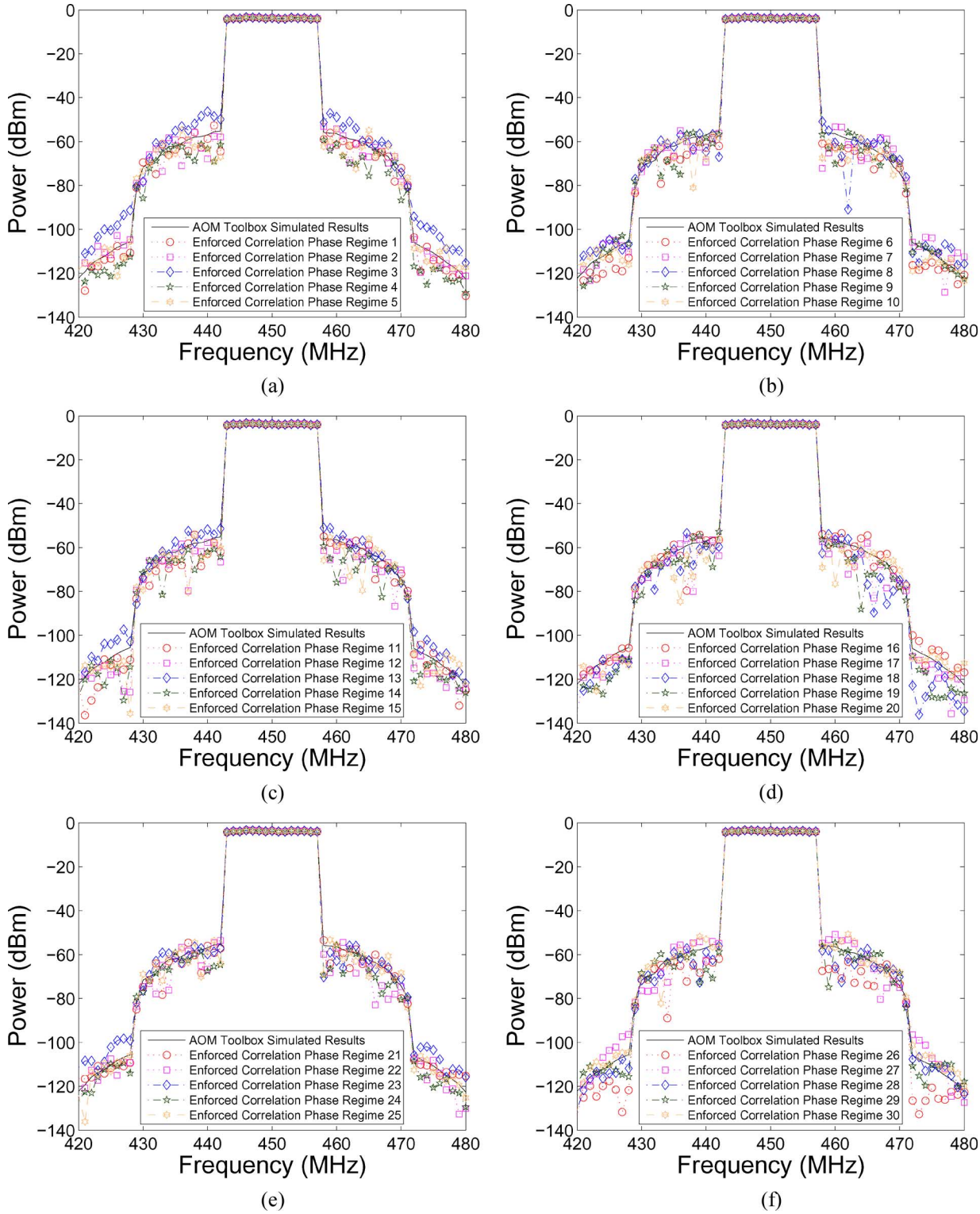

Fig. 5. Results of 30 enforced correlation simulations with results from uncorrelated phase simulation for reference. (a) Enforced correlation phase regimes 1–5. (b) Enforced correlation phase regimes 6–10. (c) Enforced correlation phase regimes 11–15. (d) Enforced correlation phase regimes 16–20. (e) Enforced correlation phase regimes 20–25. (f) Enforced correlation phase regimes 26–30.

upon uncorrelated phase input tones in their computational engines. Such environments compute the average power at a particular frequency by forming a vectorial sum of phasors and then squaring the magnitude of the resulting phasor. When the phases of the input tones are considered to be independent and identically distributed random variables, their joint probability distribution will tend to be Gaussian distributed, and thus, the ensemble average of the output of 30 simulations can be considered to give definitive results [35]. Thus, a total of 30 separate simulations in a computational engine that enforced correlation were run in order to perform this comparison. Each simulation used a randomly selected set of 15 phases or phase regimes, and

Authorized licensed use limited to: North Carolina State University. Downloaded on February 2, 2009 at 13:52 from IEEE Xplore. Restrictions apply.

each simulation used a different phase regime. Fig. 5 shows the results of these enforced correlation simulations, with the results of five enforced correlation phase simulations shown in each plot in the figure. For comparison, the uncorrelated phase simulation results from Fig. 4 are included. Note that no single simulation result using enforced correlation is in agreement with the uncorrelated phase simulation results, and that generally there are large variations in the predicted adjacent-band power levels in each simulation result when correlation is enforced.

It is only possible for the enforced correlation simulation results—typical of those produced by HB methods—to approach the uncorrelated phase results by averaging the results of many enforced correlation simulations, effectively a form of Monte Carlo analysis. Fig. 6 shows the effect of averaging enforced correlation simulations 1–8, 1–16, and 1–30, respectively. As can be seen, there are some variations from the average uncorrelated phase power when only eight simulations are averaged. Better results are achieved from averaging 16 simulations, while averaging 30 simulations produces results nearly identical to those produced by the single uncorrelated phase simulation.

B. Narrow-Band IM Analysis Example

In this example, the stimulus consisted of 14 of the same 15 carriers used in Section IV-A. The carrier at 450 MHz was turned off, and measurements were made of the narrowband IM in the vicinity of the 450-MHz signal. Due to the narrowband nature of the measurement, it was not assumed that the carriers were set at 1-MHz nominal increments as in the previous example. Instead, two measurements were made, with the first made over a range of 442.5 to 457.5 MHz solely for the purpose of obtaining the instantaneous oscillating frequencies from the linear response. The second measurement, made immediately following the first, measured the narrowband IM over a 1.2-MHz bandwidth centered around 450 MHz. Table II shows the nominal and actual measured frequencies where the actual frequencies were those used in the AOM Toolbox environment to obtain the simulated results. Note that the measured frequencies of oscillation are not commensurate, and thus it would be challenging to perform an HB simulation using them. For example, at the 1-MHz nominal spacing, a reasonably accurate HB analysis could probably be performed with as few as 32–64 points, but when the input tones are permitted to occur at 25-kHz increments, 600 points minimum are necessary, and probably 1024 points would be used. However, the measured frequencies in Table II are handled by the AOM Toolbox with no more difficulty than the nominal ones. In the AOM Toolbox environment, 15 carrier frequencies were again considered as the input, but the amplitude of the center tone at 450 MHz was set to zero. Fig. 7 shows the results of the AOM Toolbox simulation in the narrowband region around 450 MHz. Good agreement is seen in the area above the noise floor of the measuring equipment, allowing for the fact that continuous drift (of up to 30 kHz) in the carrier frequencies of the sources results in a "fill-in" effect in the measured results, where the measurement interval is only 2 kHz. The AOM Toolbox also predicts fifth-order spectral content below the noise floor of the measuring equipment.

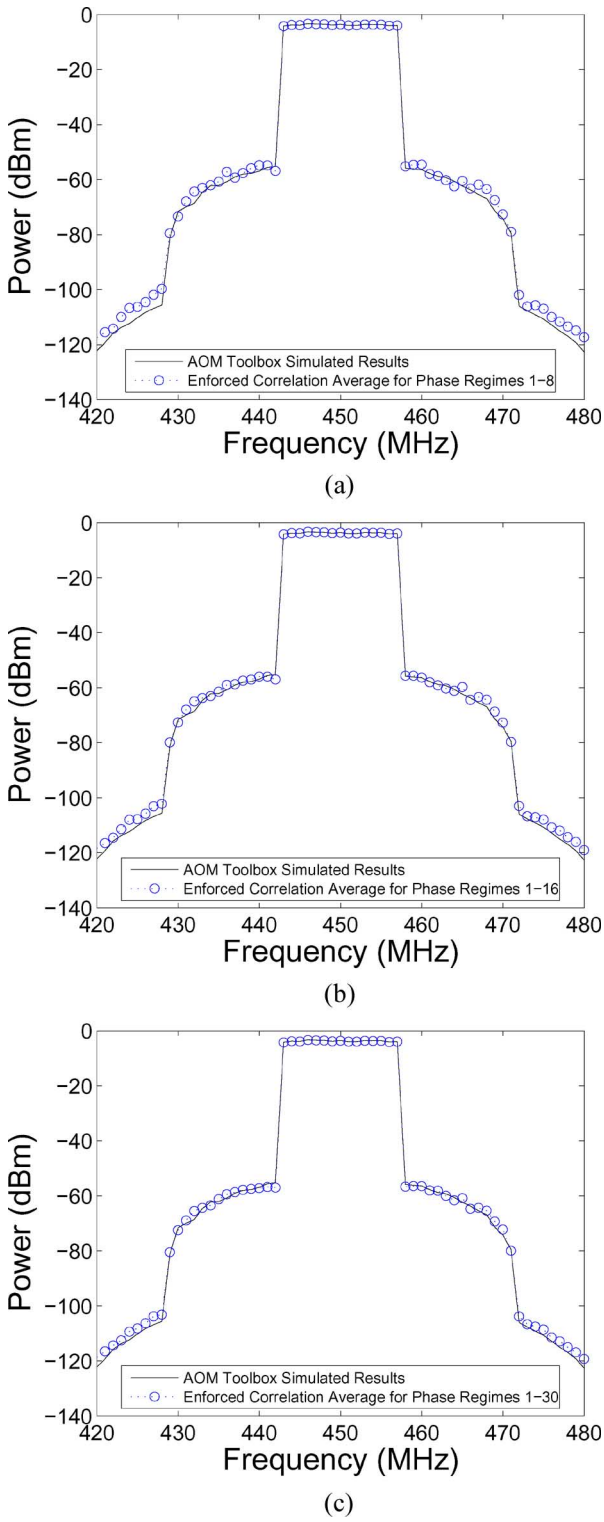

Fig. 6. Results averaging 8, 16, and 30 enforced correlation simulations. (a) Average of enforced correlation phase regimes 1–8. (b) Average of enforced correlation phase regimes 1–16. (c) Average of enforced correlation phase regimes 1–30.

Table III provides further data on the results produced by the AOM Toolbox, and here it can be seen that all of the simulated results falling below the noise floor of the measurements are comprised entirely of fifth-order spectral content.

Authorized licensed use limited to: North Carolina State University. Downloaded on February 2, 2009 at 13:52 from IEEE Xplore. Restrictions apply.

TABLE II
MEASURED FREQUENCIES OF CARRIER OSCILLATION FOR NARROWBAND IM ANALYSIS

Nominal Frequency (MHz)	Measured Frequency (MHz)	Nominal Frequency (MHz)	Measured Frequency (MHz)
443	443.000	451	451.050
444	444.000	452	452.000
445	445.000	453	452.975
456	445.950	454	453.950
447	446.975	455	454.950
448	448.000	456	455.950
449	449.050	457	456.950

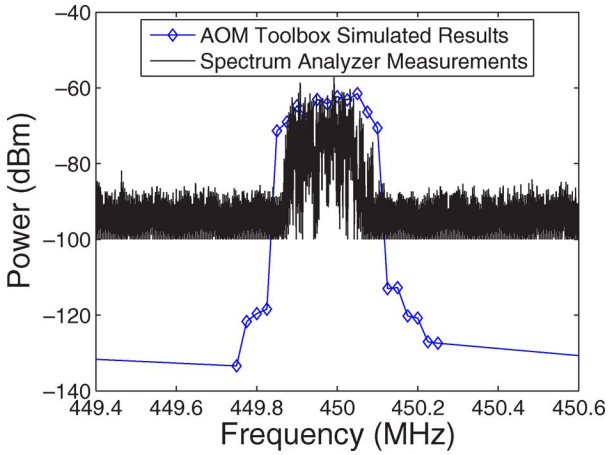

Fig. 7. Simulated and measured results for narrowband IM.

TABLE III
NUMBERS OF PHASORS AVERAGED AT IN-BAND IM FREQUENCIES

Frequency (MHz)	Simulated Power (dBm)	Number of 3rd Order Phasors	Number of 5th Order Phasors
449.750	−133.4304	0	1
449.775	−121.7008	0	2
449.800	−119.6205	0	15
449.825	−118.4364	0	17
449.850	−71.3629	1	68
449.875	−68.9911	2	67
449.900	−64.7140	7	155
449.925	−68.1083	5	152
449.950	−63.0783	12	254
449.975	−64.2181	6	234
450.000	−62.3139	12	256
450.025	−63.1690	7	185
450.050	−61.4909	13	178
450.075	−66.4031	4	96
450.100	−70.5952	4	93
450.125	−113.0054	0	42
450.150	−112.7395	0	48
450.175	−120.1977	0	12
450.200	−120.7672	0	13
450.225	−127.0383	0	3
450.250	−127.4075	0	2

TABLE IV
COSTS OF COMPUTATION IN THE AOM TOOLBOX

Computation Item	Adjacent-Band IM Computing time (sec)	Narrow-Band IM Computing time (sec)
BIPD Table	199.92	187.74
Spec. Map. Table	1217.40	1147.20
Set-Up Cost	1417.32	1334.94
Spec. Trans. Matrix	576.65	548.49
Function Evaluation	0.53	0.49
Evaluation Cost	577.18	548.98
Totals (1 run)	1994.50	1883.92

C. Computational Considerations

The use of the AOM Toolbox as a simulation environment entails two sets of computational costs. The first is a *setup tabulation* cost that includes the computation of the BIPD and spectrum mapping tables. These two tables are solely a function of the vector of input frequencies, but are independent of the amplitudes and phases of the input signals so their costs can be amortized over multiple simulations. The second type of computational cost, called the *evaluation* cost, is incurred on each execution of the environment, and includes the cost of creating the input spectral vector (negligible, thus it is omitted), the spectrum transform matrix, and the matrix–vector multiplications necessary to evaluate the nonlinear transfer function.

Table IV shows these costs in the form of time of computation on an AMD Athlon X2 4400 platform with 4 GB of DRAM running a 64-bit version of MATLAB under a Linux operating system (and with most of the CPU time devoted to MATLAB) for the two example scenarios given in Sections IV-A and B. The *setup tabulation* times of roughly 23 min dominate in both cases, but note that this cost was incurred only once in order to compute the 30 coherent phase simulations used in the adjacent-band IM modeling scenario. The *evaluation* times for both examples are between 9–10 min. The very low *function evaluation* times shown in Table IV are attributable to MATLAB's superior sparse matrix implementation and to the fact that the spectrum transform matrices for both problems were very sparse—the matrix for the adjacent-band IM example had only 0.39% nonzeros, while the matrix for the narrowband IM example had only 0.36% nonzeros. It is also worth noting that the adjacent-band IM example, in which the input signals were nominally spaced at 1-MHz intervals, had 123 276 unique BIPD table entries, but only 356 unique numerical frequencies. For the narrowband IM example, there were 123 063 unique BIPD table entries mapping to 3994 unique numerical frequencies as a result of using the more exacting measured carrier frequencies (with 25-kHz measurement increments) in lieu of the nominal 1-MHz spacing.

V. CONCLUSION

The major result of the study reported here concerns the simulation of circuits excited by multiple uncorrelated tones. A computer-aided analysis environment, the AOM Toolbox, was developed that accurately models the response of nonlinear circuits to such a stimulus in a single simulation. (For further information on the AOM Toolbox, go to http://www.freeda.org/

Authorized licensed use limited to: North Carolina State University. Downloaded on February 2, 2009 at 13:52 from IEEE Xplore. Restrictions apply.

AOM.) By creating a vector description (the BIPD table) of the frequency domain and using this underlying vector description as a further decomposition of the numerical frequency, it is possible to appropriately combine uncorrelated nonlinear interactions of the input tones to correctly model the response of the system. This is effectively done by creating and preserving uncorrelated phasor content at each order of nonlinearity as dictated by the BIPD table.

For the case of adjacent-band IM distortion modeling, it was shown that the results produced by the AOM Toolbox are essentially identical to those produced by averaging the results of multiple simulations performed using conventional techniques that enforce phase correlation of the tones. Such simulations are performed with random initial phases of the tones, and by averaging the ensemble of results of multiple simulations, the same results as a single AOM Toolbox simulation are obtained. A second example of narrowband IM distortion modeling accurately predicted the in-band IM that might be seen in cable television channel excited by IM among 14 other channels. The AOM Toolbox has proven to be useful for predicting the results of broadband and narrowband IM scenarios.

It should be noted that the transfer function used in this study was in the form of a simple polynomial, and that a rational polynomial form might not be expected to produce such conclusive results because of the necessity to invert a spectrum transform matrix (for the denominator polynomial) and left multiply it by the numerator output spectral vector, thus introducing a numerical effect akin to enforced correlation. If a transfer function in rational polynomial form is amenable to division, the resulting quotient polynomial could be effectively deployed. Another possibility might be to assure that the matrix to be inverted is strongly diagonally dominant so as to minimize any numerically enforced correlation.

This study clarifies one of the vexing issues in circuit simulation, one that becomes increasingly important when modeling systems excited by multiple tones or by digitally modulated signals approximated by multiple tones.

REFERENCES

[1] "Harmonic balance simulation," Agilent Technol., Palo Alto, CA, Aug. 2005. [Online]. Available: http://www.edasupportweb.soco.agilent.com/docs/adsdoc2005A/cktsimhb/index.html

[2] V. Rizzoli, F. Mastri, F. Sgallari, and G. Spaletta, "Harmonic-balance simulation of strongly nonlinear very large-size microwave circuits by inexact Newton methods," in *IEEE MTT-S Int. Microw. Symp. Dig.*, Jun. 1996, vol. 3, pp. 1357–1360.

[3] V. Rizzoli, C. Cecchetti, D. Masotti, and F. Mastri, "Nonlinear processing of digitally modulated carriers by the inexact-Newton harmonic balance technique," *Electron. Lett.*, vol. 33, no. 21, pp. 1760–1761, Oct. 9, 1997.

[4] V. Rizzoli, A. Neri, F. Mastri, and A. Lipparini, "A Krylov-subspace technique for the simulation of integrated RF/microwave subsystems driven by digitally modulated carriers," *Int. J. RF Microw. Comput.-Aided Eng.*, vol. 9, no. 6, pp. 490–505, Nov. 1999.

[5] V. Rizzoli, A. Lipparini, D. Masotti, and F. Mastri, "Efficient circuit-level analysis of large microwave systems by Krylov-subspace harmonic balance," in *IEEE MTT-S Int. Microw. Symp. Dig.*, May 2001, vol. 1, pp. 25–28.

[6] W. Ciciora, J. Farmer, D. Large, and M. Adams, *Modern Cable Television Technology*, 2nd ed. San Mateo, CA: Morgan Kauffman, 2004.

[7] K. Naishadham, "Characterization of intermodulation distortion in multicarrier transmission systems," in *IEEE MTT-S Int. Microw. Symp. Dig.*, Jun. 2002, vol. 3, pp. 2193–2196.

[8] J. H. Haywood and Y. L. Chow, "Intermodulation distortion analysis using a frequency-domain harmonic balance technique," *IEEE Trans. Microw. Theory Tech.*, vol. 36, no. 8, pp. 1251–1257, Aug. 1988.

[9] C. R. Chang, M. B. Steer, and G. W. Rhyne, "Frequency-domain spectral balance using the arithmetic operator method," *IEEE Trans. Microw. Theory Tech.*, vol. 37, no. 11, pp. 1681–1688, Nov. 1989.

[10] C. R. Chang and M. B. Steer, "Frequency-domain nonlinear microwave simulation using the arithmetic operator method," *IEEE Trans. Microw. Theory Tech.*, vol. 38, no. 8, pp. 1139–1143, Aug. 1990.

[11] J. Rutkowski, E. Limiti, B. Galwas, and L. Scucchia, "Frequency-domain spectral balance method of nonlinear analysis of microwave circuits," in *MIKON-94 10th Int. Microw. Conf.*, Ksiaz Castle, Poland, 1994, pp. 315–318.

[12] F. Giannini, G. Leuzzi, E. Limiti, and L. Scucchia, "Non-linear frequency-domain analysis of microwave circuits through rational functions modelling," in *Proc. 26th Eur. Microw. Conf.*, Swanley, U.K., 1996, vol. 2, pp. 551–554, Nexus.

[13] D. Schreurs, J. Rutkowski, A. Beyer, and B. Nauwelaers, "Development of a frequency-domain simulation tool and nonlinear device model from vectorial large-signal measurements," *Int. J. RF Microw. Comput.-Aided Eng.*, vol. 10, no. 1, pp. 63–72, Jan. 2000.

[14] N. B. de Carvalho and J. C. Pedro, "Simulating strong non-linear microwave circuits driven by a large number of input tones," in *27th Eur. Microw. Conf./Exhibition*, 1997, vol. 2, pp. 820–825.

[15] N. B. de Carvalho and J. C. Pedro, "Multitone frequency-domain simulation of nonlinear circuits in large- and small-signal regimes," *IEEE Trans. Microw. Theory Tech.*, vol. 46, no. 12, pp. 2016–2024, Dec. 1998.

[16] N. B. de Carvalho and J. C. Pedro, "Simulation of multi-tone IMD distortion and spectral regrowth using spectral balance," in *IEEE MTT-S Int. Microw. Symp. Dig.*, Jun. 1998, vol. 2, pp. 729–732.

[17] N. B. de Carvalho and J. C. Pedro, "Non-linear circuit simulation of complex spectra in the frequency domain," in *IEEE Int. Electron., Circuits, Syst. Conf.*, Sep. 1998, vol. 1, pp. 129–132.

[18] J. C. Pedro and N. B. de Carvalho, "On the use of multitone techniques for assessing RF components' intermodulation distortion," *IEEE Trans. Microw. Theory Tech.*, vol. 47, no. 12, pp. 2393–2402, Dec. 1999.

[19] J. F. Hart, *Computer Approximations*. New York: Wiley, 1968.

[20] I. Koren and O. Zinaty, "Evaluating elementary functions in a numerical coprocessor based on rational approximations," *IEEE Trans. Comput.*, vol. 39, no. 9, pp. 1030–1037, Aug. 1990.

[21] J. R. Gilbert, C. Moler, and R. Schreiber, "Sparse matrices in MATLAB: Design and implementation," *SIAM J. Matrix Anal. Applicat.*, vol. 13, no. 1, pp. 333–356, Jan. 1992.

[22] D. D. Weiner and J. E. Spina, *Sinusoidal Analysis and Modeling of Weakly Nonlinear Circuits*. New York: Van Nostrand, 1980.

[23] N. Morrison, *Introduction to Fourier Analysis*. New York: Wiley, 1994.

[24] A. Tucker, *Applied Combinatorics*, 4th ed. New York: Wiley, 2002.

[25] F. P. Hart, D. G. Stephenson, C. R. Chang, K. Gharaibeh, R. G. Johnson, and M. B. Steer, "Mathematical foundations of frequency-domain modeling of nonlinear circuits and systems using the arithmetic operator method," *Int. J. RF Microw. Comput.-Aided Eng.*, vol. 13, no. 6, pp. 473–495, Nov. 2003.

[26] C. R. Chang, "Computer-aided analysis of nonlinear microwave analog circuits using frequency-domain spectral balance," Ph.D. dissertation, Dept. Elect. Eng. Comput. Sci., North Carolina State Univ., Raleigh, NC, 1990.

[27] C. D. Meyer, *Matrix Analysis and Applied Linear Algebra*. Philadelphia, PA: SIAM, 2000.

[28] A. V. Oppenheim, A. W. Willsky, and I. T. Young, *Signals and Systems*. New York: Prentice-Hall, 1983.

[29] A. V. Oppenheim, "Generalized superposition," *Inform. Control*, vol. 11, no. 5/6, pp. 528–536, Nov.–Dec. 1967.

[30] B. Razavi, "A study of injection locking and pulling in oscillators," *IEEE J. Solid-State Circuits*, vol. 39, no. 9, pp. 1415–1424, Sep. 2004.

[31] "ZHL-5W-1 datasheet, ver. M98142," Mini-Circuits, CITY, STATE/COUNTRY, May 17, 2005. [Online]. Available: http://www.minicircuits.com/pdfs/ZHL-5W-1.pdf

[32] A. L. Walker, "Behavioral modeling and characterization of nonlinear operation in RF and microwave systems," Ph.D. dissertation, Dept. Elect. Eng. Comput. Sci., North Carolina State Univ., Raleigh, NC, 2005.

[33] A. Walker, M. B. Steer, and K. G. Gard, "Application of large signal vector intermodulation analyzer to behavioral modeling of nonlinear microwave circuits with memory effect," *IEEE Trans. Microw. Theory Tech.*, vol. 54, no. 5, pp. 1991–1999, May 2006.

Authorized licensed use limited to: North Carolina State University. Downloaded on February 2, 2009 at 13:52 from IEEE Xplore. Restrictions apply.

[34] *Composite Distortion Measurements (CSO & CTB)*, Amer. Nat. Standard ANSI/SCTE 06 1999R2004, Soc. Cable Telecommun. Eng., Exton, PA, 2004.
[35] Y. Viniotis, *Probability and Random Processes For Electrical Engineers*. New York: WCB McGraw-Hill, 1998.

Frank P. Hart (S'06–M'07) received the Bachelor of electrical engineering degree (*cum laude*) from the University of Delaware, Newark, in 1984, the M.S.E.E. degree from North Carolina State University, Raleigh, in 1994, and is currently working toward the Ph.D. degree at North Carolina State University.

He is currently a Research Assistant with the Electronics Research Laboratory, North Carolina State University. From 1984 to 1995, he was with the IBM Corporation, Research Triangle Park, NC, where he was involved with telecommunications networking and notebook personal computer hardware development. During his years with the IBM Corporation, he was promoted several times, rising to the level of Advisory Engineer before his departure. From 1995 to 2001, he was with the Intel Corporation, first with their Hillsboro, OR location, and later with their Santa Clara, CA location, here he was involved with the development of "mobile module" subassemblies for notebook computers and mobile chipset architecture definition. At the time of his departure from the Intel Corporation, he was a Senior Staff Engineer. He has coauthored three papers and a book chapter. He coholds 12 patents.

Michael B. Steer (S'76–M'82–SM'90–F'99) received the B.E. and Ph.D. degrees in electrical engineering from the University of Queensland, Brisbane, Australia, in 1976 and 1983, respectively.

He is currently the Lampe Professor of Electrical and Computer Engineering with North Carolina State University, Raleigh. In 1999 and 2000, he was Professor with the School of Electronic and Electrical Engineering , The University of Leeds, where he held the Chair in Microwave and Millimeter-Wave Electronics. He was also Director of the Institute of Microwaves and Photonics, The University of Leeds. He has authored over 360 publications on topics related to RF, microwave and millimeter-wave systems, high-speed digital design, and RF and microwave design methodology and circuit simulation. He coauthored *Foundations of Interconnect and Microstrip Design* (Wiley, 2000).

Prof. Steer is active in the IEEE Microwave Theory and Technique Society (IEEE MTT-S). In 1997, he was secretary of the IEEE MTT-S, and from 1998 to 2000, he was an elected member of the IEEE MTT-S Administrative Committee (AdCom). He was the Editor-in-Chief of the IEEE TRANSACTIONS ON MICROWAVE THEORY AND TECHNIQUES (2003–2006). He was a 1987 Presidential Young Investigator (USA). In 1994 and 1996, he was the recipient of the Bronze Medallion presented by the U.S. Army Research Office for "Outstanding Scientific Accomplishment." He was also the recipient of the Alcoa Foundation Distinguished Research Award presented by North Carolina State University in 2003.

Authorized licensed use limited to: North Carolina State University. Downloaded on February 2, 2009 at 13:52 from IEEE Xplore. Restrictions apply.